

This is a repository copy of *CD4+ 1 T cells alter the stromal microenvironment and repress medullary erythropoiesis in murine visceral leishmaniasis.*

White Rose Research Online URL for this paper:

<https://eprints.whiterose.ac.uk/id/eprint/139480/>

Version: Accepted Version

Article:

Preham, Olivier Yvon Giuseppe, Pinho, Flaviane Alves, Pinto, Ana Isabel orcid.org/0000-0002-9640-6333 et al. (5 more authors) (2018) CD4+ 1 T cells alter the stromal microenvironment and repress medullary erythropoiesis in murine visceral leishmaniasis. *Frontiers in immunology*. 2958. ISSN: 1664-3224

<https://doi.org/10.3389/fimmu.2018.02958>

Reuse

This article is distributed under the terms of the Creative Commons Attribution (CC BY) licence. This licence allows you to distribute, remix, tweak, and build upon the work, even commercially, as long as you credit the authors for the original work. More information and the full terms of the licence here:

<https://creativecommons.org/licenses/>

Takedown

If you consider content in White Rose Research Online to be in breach of UK law, please notify us by emailing eprints@whiterose.ac.uk including the URL of the record and the reason for the withdrawal request.

**CD4⁺ T cells alter the stromal microenvironment and repress
medullary erythropoiesis in murine visceral leishmaniasis.**

**Olivier Preham^{1^}, Flaviane A. Pinho^{2&}, Ana Pinto¹, Gulab Fatima Rani¹, Najmeeyah
Brown¹, Ian S. Hitchcock¹, Hiro Goto² and Paul M. Kaye^{1*}**

¹Centre for Immunology and Infection, Dept of Biology and Hull York Medical School,
University of York, Heslington, York, YO10 5DD, UK

²Laboratório de Soroepidemiologia e Imunobiologia, Instituto de Medicina Tropical de São
Paulo, and Faculdade de Medicina, Universidade de São Paulo, São Paulo, Brazil

[^] Current address: UCL Institute of Immunity and Transplantation, Royal Free Hospital,
London, NW3 2QG

[&]Current address: Escola de Medicina Veterinária e Zootecnia, Universidade Federal da
Bahia, Salvador, BA, Brazil, 40170-110

Running title: CD4⁺ T cell repression of erythropoiesis during visceral leishmaniasis.

Keywords: erythropoiesis; stromal cells; macrophages; bone marrow; leishmaniasis.

***Correspondence to:** Prof. Paul M Kaye

paul.kaye@york.ac.uk

Abstract

Human visceral leishmaniasis, a parasitic disease of major public health importance in developing countries, is characterized by variable degrees of severity of anemia, but the mechanisms underlying this change in peripheral blood have not been thoroughly explored. Here, we used an experimental model of visceral leishmaniasis in C57BL/6 mice to explore the basis of anemia following infection with *Leishmania donovani*. 28 days post infection, mice showed bone marrow dyserythropoiesis by myelogram, with a reduction of TER119⁺ CD71^{-/+} erythroblasts. Reduction of medullary erythropoiesis coincided with loss of CD169^{high} bone marrow stromal macrophages and a reduction of CXCL12-expressing stromal cells. Although the spleen is a site of extramedullary erythropoiesis and erythrophagocytosis, splenectomy did not impact the extent of anemia or affect the repression of medullary hematopoiesis that was observed in infected mice. In contrast, these changes in bone marrow erythropoiesis were not evident in B6.*Rag2*^{-/-} mice, but could be fully reconstituted by adoptive transfer of IFN γ -producing but not IFN γ -deficient CD4⁺ T cells, mimicking the expansion of IFN γ -producing CD4⁺ T cells that occurs during infection in wild type mice. Collectively, these data indicate that anemia during experimental murine visceral leishmaniasis can be driven by defects associated with the bone marrow erythropoietic niche, and that this represents a further example of CD4⁺ T cell-mediated immunopathology affecting hematopoietic competence.

Introduction

The bone marrow (BM) is the main site of hematopoiesis in adult mammals and occurs within the cavities of long bones. Hematopoiesis is a complex process through which hematopoietic stem cells (HSCs) proliferate and differentiate into mature blood cells and is largely restricted to specific microenvironments or “niches” that are comprised of a variety of non-hematopoietic stromal cells and secreted factors. The stromal cell-derived chemokine CXCL12 and its receptor CXCR4 are responsible for the retention of HSCs in the BM. Disruption of the CXCL12-CXCR4 axis, or depletion of CXCL12-abundant reticular (CAR) cells, mobilizes HSCs in the peripheral blood [1]. A wide spectrum of diseases impact on hematopoiesis in general and on erythropoiesis in particular by altering these niches, including myeloproliferative neoplasms and infectious diseases [2]. For example, *Escherichia coli* and *Anaplasma phagocytophilum* infections in murine models has been shown to induce CXCL12 down-regulation in the BM and subsequent HSC mobilization [3, 4]. The development of anemia is often complex and multifactorial, as evidenced by experimental studies in infectious disease models and often reflects a balance between erythropoiesis and erythrocyte clearance. For example, in *Trypanosoma brucei* infection, anemia is in part caused by nitric oxide (NO) production, and pro-inflammatory cytokines such as IFN γ and TNF positively correlate with anemia severity [5]. In contrast, direct lysis of RBC is seen during acute malaria [6]. CD169⁺ BM stromal macrophages are also an essential component of the niche for erythropoiesis [7] as well as important regulators of stromal cells within the HSC niche [8, 9], but less is known about how their function is impacted during infection, or in relation to the development of anemia.

Hematological disturbances are a hallmark of human and canine visceral leishmaniasis (VL) [10, 11], caused by infection with the protozoan parasites *Leishmania donovani* or *L.*

69 *infantum*. Differing degrees of cytopenia are associated with disease stage, and as risk
70 factors for VL-related death [12, 13]. VL often results in pancytopenia [14-16] and may
71 sometimes be misdiagnosed as another hematological disorder, such as myelodysplastic
72 syndrome [17]. Various mechanisms have been proposed to underpin the development of
73 VL-associated pancytopenia, including auto-immune destruction of erythrocytes, platelets
74 and leukocytes, or BM failure [18]. Anemia has been attributed to aberrant
75 sialoglycosylation of red blood cells [19], altered recognition of band 3 subsequent to
76 oxidative stress [20] or enhanced macrophage-mediated erythrophagocytosis [21].

77
78 While the immune response and hematological consequences of VL have been extensively
79 studied, far less is known about the regulation of hematopoiesis per se during disease, in part
80 due to the ethical challenges involved in studying this in humans. Hematopoiesis has been
81 examined in a hamster model of VL [22], with the finding that *L. donovani* infection induces
82 apoptosis in erythropoietic progenitors in the BM. However, lack of tools for dissecting the
83 hamster immune and hematopoietic microenvironment poses challenges in exploiting this
84 model. Although the mouse model of VL is not lethal, it has been extensively studied to
85 provide more mechanistic data on immunity and immunopathology [23, 24]. However, this
86 model has to date been poorly utilized in the study of hematological dysfunction. Cotterell et
87 al. demonstrated that chronic VL in BALB/c mice results in an increase of hematopoietic
88 progenitors in the spleen and the BM [25], and that BM stromal macrophage-derived cells
89 may become more supportive of myelopoiesis after infection with *L. donovani* in vitro, due to
90 increased secretion of GM-CSF and TNF [26]. More recently, alterations in the HSC
91 compartment have been described that might contribute both to ongoing VL-associated
92 immunosuppression [27] and to long term hematopoietic competence [28].

Here, we have focused on exploring the mechanisms underpinning anemia in C57BL/6 mice infected with *L. donovani*. We show that infected mice develop BM dyserythropoiesis, evidenced both by myelogram and by a reduction of medullar TER119⁺ CD71^{-/+} erythroblasts. Reduction of medullary erythropoiesis coincided with loss of CD169^{high} stromal macrophages and a reduction of CXCL12-expressing stromal cells. We demonstrate, through the use of immunodeficient B6.*Rag2*^{-/-} mice and adoptive cell transfer, that all of these events strictly require the presence of CD4⁺ T cells expressing IFN γ . Hence, we propose that repression of medullary erythropoiesis is added to the catalogue of immunopathological sequelae associated with *Leishmania donovani* infection.

Material and methods

Ethics statement

All animal care and experimental procedures were performed under UK Home Office License (Ref # PPL 60/4377) and with approval from the Animal Welfare and Ethical Review Board of the Department of Biology, University of York.

Mice

C57BL/6, B6.*Rag2*^{-/-}, B6.*Cxcl12*^{tm2.1Sjm/J} mice (Jackson Laboratories) and B6.hCD2-DsRed mice were bred at the University of York. IFN γ -KO (B6.129S7-*Ifng*^{tm1Ts/J}, stock no. 002287) mice were obtained from the Jackson Laboratory. All mice were maintained under specific pathogen-free conditions (FELASA 67M standard). As appropriate, mice were micro-chipped, randomly allocated to groups and infected intravenously with 2-3x10⁷ *L. donovani* (LV9) amastigotes isolated from the spleen of infected B6.*Rag2*^{-/-} mice. Mice were splenectomized (Sp_x) or sham-operated by a commercial supplier (Charles River UK), and

were allowed to recover for 3 weeks before being infected. As required, 6×10^5 sort-purified splenic $CD45^+CD4^+CD3^+CD8^-B220^-TCR\gamma\delta^-CD49b^-$ cells derived from wild type or IFN γ -KO mice were transplanted into B6.*Rag2*^{-/-}.CD45.1Cg recipient mice 24h prior to infection. Unless stated otherwise, experimental mice were killed by cervical dislocation four weeks after infection.

Blood analysis

Blood was collected from terminally anaesthetized mice by cardiac puncture in syringes coated with Citrate-dextrose and transferred into a EDTA-coated Vacutainer®. Blood analysis was performed with a Hemavet 950FS (Drew Scientific)

Bone marrow myelogram

BM samples were obtained by aspiration biopsy from iliac crest using 24 G needle attached to a 5mL disposable plastic syringe with 10% EDTA and smears were stained with May-Grünwald Giemsa (Lewis et al., 2006). Samples were then re-coded for blind analysis. A differential count of 500 cells was made in BM smears to calculate: myeloid : erythroid (M:E) ratio, the myeloid maturation ratio, the erythroid maturation ratio, myeloid precursor cells (myeloblasts + promyelocyte + myelocyte), percentages of myeloid mature cells (metamyelocyte + band neutrophils + segmented neutrophils), erythroid precursor cells (CD71⁺TER119^{lo} proerythroblasts + CD71^{-/+}TER119^{high} basophil erythroblasts), erythroid mature cells (polychromatic erythrocyte + orthochromatic erythrocytes; equivalent to CD71^{-/+}TER119^{high}), monocytes, macrophages, plasma cells and megakaryocytes according to Yang et al. [40]. The dysplastic features were also analyzed in the myeloid and erythroid series and in megakaryocytes.

144 *Immunohistochemistry*

145 Femurs were isolated and cleaned to remove excessive tissue then fixed overnight at 4°C in
146 periodate-lysine-paraformaldehyde fixative (10mM sodium periodate dissolved in three parts
147 0.1M lysine-HCl 0.1M Na₂HPO₄ and one part 20% (w/v) paraformaldehyde) and decalcified
148 for 3 days at 4°C with slow agitation in 10% EDTA, 0.1M Tris, pH6.95. Bones were
149 transferred in 30% sucrose in PBS for a final overnight incubation at 4°C. Spleen and bones
150 were embedded in Optimal Cutting Temperature (OCT™) compound (Tissue-Tek) in
151 Cryomolds® (Tissue-Tek) and snap-frozen on dry ice. Spleen and femoral 5µm-sections
152 were cut using a CM1900 cryostat (Leica Microsystems) onto Polysines® slides (Thermo
153 Fisher). Spleen section were fixed in ice-cold acetone for 10min on the day of staining.
154 Sections were blocked in staining buffer (PBS, 0.05% (w/v) BSA, 5% goat serum) for 1h at
155 RT. Excess buffer was removed and slides stained with fluorochrome-labelled TER119,
156 F4/80, CD71 or isotype controls (eBioscience) in staining buffer for 1h at RT or overnight at
157 4°C. Slides were washes three times for 5min in washing buffer (PBS 0.05% (w/v) BSA) and
158 counterstained with DAPI. Section were mounted in ProLong® Gold antifade reagent (Life
159 Technologies) and sealed before imaging. Confocal images were obtained using LSM780 or
160 LSM710 systems (Leica Microsystems) and analyzed using Zen software (Carl Zeiss).
161 Samples were assessed blind to treatment group.

162

163 *Flow cytometry*

164 Spleen cells were dissociated using a 70µm cell strainer. Femurs were cut at both ends to
165 expose the bone cavity and the BM was flushed with PBS 1% FCS (flow cytometry buffer)
166 using a 25-gauge needle through a 70µm cell strainer. Single cell suspensions were washed
167 (5min at 300g) and red blood cells were lysed with ACK buffer (5min at RT). Nucleated cells

were subsequently counted using a Vi Cell XR Cell Counter (Beckman Coulter). Cell suspensions were incubated in FcBlock (mouse CD16/32 purified antibody, clone 93) prior to staining with antibodies specific for CD71 (clone R17217), TER119 (clone TER-119), and CD45 (clone 30-F11) or with F4/80 (clone BM8), Ly-6G (clone Gr-1), CD115 (clone AFS98) and CD169 (clone SER-4). For T cell characterization, cells were labeled with in optimized concentration of flurochrome-labelled CD45, CD4 (clone RM4-5 or GK1.5), CD8 (clone 53-7.7), TCR $\gamma\delta$ (clone GL-3), B220 (CD45R; clone RA3-6B2)), CD49d (clone DX-5) and CD3 (clone 145-2C11) antibodies diluted in 1x PBS 1% FCS and left at 4°C for 30 min in the dark. Cells were washed and analyzed on a Cyan flow cytometer (Beckman Coulter).

Statistical Analysis

Data were analyzed using GraphPad Prism 5.0 (Prism Software, Irvine, CA, USA). When comparing two groups, Student's t-test or Mann-Whitney test was used according to the data distribution. Welch's correction was applied for the Student's t-test in cases of unequal variances between the two groups. For multiple comparison, one-way ANOVA or Kruskal-Wallis tests were used according to the data distribution followed by Turkey's or Dunn's multiple comparison tests, respectively. Downstream analyses were performed blind to treatment group.

Results

C57BL/6 mice were infected with *L. donovani* amastigotes by the intravenous route and blood parameters were measured over time. Data from naïve mice (n=14) were used to calculate the reference interval, or normal range, for each parameter in the complete blood count. Anemia was first evident at week 4 post infection (**Table 1 and S1 Table**), a time that

also represents the approximate peak of infection in spleen and bone marrow [28]. The mean red blood cell (RBC) count per μl of blood was 19% lower in infected mice compared to their naïve counterparts. 70% of infected mice had RBC counts below the normal range. Similarly, the mean hemoglobin (Hb) content in the blood of infected mice was decreased by $\sim 15\%$ in infected mice and $\sim 30\%$ of infected mice had Hb levels below the reference interval. The average volume of erythrocytes was unchanged, with a mean corpuscular volume (MCV) of 51 femtoliter (fl) in both groups but 3/13 infected mice (23%) had developed a macrocytic anemia. Although the overall hemoglobin concentration was reduced, all individual mice had mean corpuscular hemoglobin (MCH) values within the normal range. Blood film examination indicated the presence of aberrant red cell morphology with anisopoikilocytosis, polychromasia, acanthocytes and nucleated red cells (**S1 Fig.**). No significant change in circulating lymphocytes, granulocytes or monocytes was measured between naïve and infected mice, except for a single infected mouse that presented with both lymphopenia and eosinophilia. Thrombocytopenia was evident. These results all point towards development of a normochromic anemia coupled with thrombocytopenia as the most common hematological consequences of *L. donovani* in C57BL/6 mice.

Compensatory extra-medullary erythropoiesis occurs in the spleen but medullary erythropoiesis is repressed during EVL

Decrease in hematocrit can be caused by reduced numbers of circulating erythrocytes, by impairment of erythropoiesis or by peripheral destruction of RBC. Others have previously reported erythrophagocytosis occurring in the spleen during experimental VL [21], associated with splenomegaly. However, the spleen is also well-known as a site with a propensity for extramedullary hematopoiesis. We confirmed that splenomegaly was associated with extramedullary erythropoiesis (**Fig. 1**), as determined by an increased frequency (**Fig. 1C and D**)

and absolute number (**Fig. 1E and F**) of CD45⁻CD71^{high}TER119^{low} pro-erythroblasts and CD45⁻CD71^{high/low}TER119^{high} erythroblasts [29]. CD71⁺TER119⁺ cells localized predominantly within the enlarged red pulp (**Fig. 1G**). Hence, during experimental VL, splenomegaly provides both an environment in which splenic clearance of RBCs can occur [21], as well as an environment conducive to enhanced compensatory erythropoiesis.

To determine how anemia and medullary erythropoiesis were altered in the presence or absence of a spleen, we next compared the BM of splenectomized and sham-operated C57BL/6 mice. Decolouration of the femurs was observed in the presence and to a lesser extent in the absence of a spleen (**Fig. 2A**). Likewise, hematocrit as a measure of anemia was significantly reduced independently of the presence or absence of a spleen (**Fig. 2B**). We then stained femur sections with TER119. Nucleated TER119⁺ cells were clearly reduced in the BM of infected mice as determined by confocal microscopy (**Fig. 2C and D**). In contrast to spleen, flow cytometry with CD71 and TER119 indicated that the number of pro-erythroblasts (CD71⁺TER119^{low} cells) in BM was similar between naïve and infected mice (0.32±0.08 vs 0.28±0.06) whereas the number of erythroblasts (CD71^{-/+}TER119^{high} cells) in infected mice was significantly reduced compared to the naïve mice (2.66±0.16 vs 0.55±0.14; **Fig. 2E and F**). A similar change in erythroblast number was also observed in mice splenectomized prior to infection. Prior to day 28 p.i, we observed no significant alteration in the frequency of BM erythroid precursors (**S2 Fig**). Taken together with the data reported in Pinto et al [28], showing that infection does not affect the absolute number or frequency of myeloid-erythroid progenitors (MEPs) in bone marrow, our data suggest that only the final stages of BM erythropoiesis are impaired in *L. donovani*-infected mice, and that this occurs independently of splenomegaly and splenic function.

243 *Myelogram of BM*

244 To further characterize changes in cellularity of the BM, myeloid and erythroid cells were
245 analyzed by differential counting (**Table 2**). Infected mice had an increased myeloid:
246 erythroid ratio. Notably, infected mice had an increase in the index of myeloid maturation
247 compared to naïve mice, characterized by a high frequency of immature myeloid cells with a
248 decrease in mature myeloid cells. A significant reduction of enucleated mature erythroid
249 cells was also observed, suggesting disturbance in the maturation process and consistent with
250 the anemia observed in blood. In contrast, the frequency of lymphocytes and macrophages
251 was elevated. By morphology, alterations suggestive of dysplasia in the myeloid and
252 erythroid series, including maturation asynchrony (nuclei : cytoplasm asynchrony), giant
253 band cell, megalocyte, fragmented nuclei, binucleated cells and/or bilobed nuclei and atypical
254 mitosis were all observed in infected mice. Other findings included emperipolesis and leuco-
255 erythrophagocytosis (**S3 Fig.**)

257 *The bone marrow microenvironment is altered during EVL*

258 To focus more specifically on cellular changes associated with erythropoiesis, we next
259 examined two major components of the erythropoietic niche, stromal macrophages and
260 CXCL12-abundant reticular (CAR) cells. CD169⁺ BM stromal macrophages have been
261 reported by others to be important for supporting the later stages of erythropoiesis⁷ and are
262 identified as Gr-1⁻ CD115⁻ F4/80⁺ low side scatter (SSC^{low}) cells [7] with surface expression
263 of CD169 (**Fig. 3A and B**). In naïve mice, CD169^{low} and CD169^{high} stromal macrophages
264 could be clearly resolved (**Fig. 3B**). Although the total number of Gr-1⁻ CD115⁻ F4/80⁺
265 SSC^{low} macrophages was similar between infected and naïve mice (**Fig. 3C**), the ratio of
266 CD169^{low} : CD169^{high} populations was significantly altered. In naïve mice, CD169^{low}
267 macrophages accounted for 2.77±0.59% of bone marrow cells or ~5.x10⁵ cells per

femur/tibia, whereas CD169^{high} stromal macrophages accounted for 1.70±0.29% of total bone marrow cells (~3.5x10⁵ per femur/tibia). In contrast, in infected mice a clear population of CD169^{high} stromal cells was not apparent (**Fig. 3B**), and numbers of cells gated as positive for CD169 expression was reduced to 2.14x10⁵ per femur/tibia (**Fig. 3C**). These data suggest that either there is a loss of CD169 expression by BM stromal macrophages as a consequence of the environment created by infection, or that these cells are lost and replaced in equivalent numbers by other macrophages that lack CD169. The latter is consistent with the evidence provided above of enhanced BM myelopoiesis (**Table 2**).

CD169⁺ stromal macrophages are known to interact with stromal reticular cells that produce CXCL12 (CAR cells) and that these are composed of mesenchymal stem and progenitor cells MSPCs [30]. Therefore, we examined expression of CXCL12 at both protein and mRNA levels. RT-qPCR analysis of total BM cells from chronically infected C57BL/6 mice indicated a 50% reduction in *Cxcl12* mRNA accumulation compared to naïve mice (**Fig. 4A**). We next used CXCL12 reporter mice to identify and quantitate CAR cells expressing this chemokine. By confocal microscopy, there was a clear reduction in the frequency of cells expressing CXCL12 in infected compared to naïve mice (**Fig. 4B**). As the extensive ramifications of these cells made quantification difficult, we performed flow cytometry to validate these data (**Fig. 4C and D**). In naïve B6.*Cxcl12*^{DsRed} mice, the frequency of CAR cells was 0.32±0.02% of total bone marrow cells, corresponding to 4.84±0.49x10⁴ cells per femur/tibia. In contrast, the frequency and absolute number of Ds-Red⁺ cells were reduced in infected mice (0.11±0.01% and 1.36±0.20x10⁴ cells per femur) (**Fig. 4E and F**). Finally, to provide a functional confirmation of reduced numbers of CAR cells, we made use of the property of these cells to generate adherent fibroblastic colonies (CFU-F) *in vitro* [31]. We found a reduction in the absolute number of CFU-F in the BM of infected mice (from

32.6±3.4 CFU-F / 1x10⁶ BM cells to 11.8±4.5 CFU-F / 1x10⁶ BM cells in naïve and infected mice, respectively; **Fig. 4G**). Taken together, these results suggest that mice infected with *L. donovani* have reduced levels of stromal cell support for late-stage erythropoiesis in the BM.

Bone marrow failure is linked to the adaptive immune response

In addition to being a site of hematopoiesis, the BM is also a site of *L. donovani* infection [25, 28]. To determine whether cell mediated immunity impacted on medullary erythropoiesis, we first assessed the number of lymphocytes in the BM of infected mice. As previously described [28], both CD4⁺ and CD8⁺ T cells were found to accumulate in the BM of infected mice, though an expansion in the frequency of CD4⁺ T cells represented the major change observed (**Fig. 5A** and **S4 Figure**). Accumulation of T cells was also confirmed by confocal microscopy of femur sections in B6.hCD2-GFP mice (**Fig. 5B**). In contrast, we observed no change in the frequency of CD1b⁺ cells and a compensatory decrease in the frequency of B cells. Of note, similar changes were also observed in mice which had undergone splenectomy prior to infection, indicating that the spleen plays a limited role in the accumulation of bone marrow-homing T cells during infection (**Fig. 5A**).

We next examined erythropoiesis in the BM of B6.*Rag2*^{-/-} mice by flow cytometry to determine whether adaptive immunity played a role in the suppression of medullary erythropoiesis. As in wild type mice, B6.*Rag2*^{-/-} mice infected with *L. donovani* had similar numbers of pro-erythroblasts as control uninfected mice (**Fig. 5C**), despite significantly higher systemic parasite burden (**S5 Fig.**). In contrast, whereas wild type mice had significantly reduced numbers of erythroblasts, only a modest and not significant reduction in these cells was observed in infected B6.*Rag2*^{-/-} mice (**Fig. 5D**). Similarly, B6.*Rag2*^{-/-} mice showed no reduction of *Cxcl12* mRNA accumulation after 4 weeks of infection compared to

the ~50% reduction seen in wild-type mice (**Fig. 5E**). In addition, there was no change in the expression of CD169^{high} on Gr-1⁻ CD115⁻ F4/80⁺ SSC^{low} bone marrow macrophages (**Fig. 5F**), and the ratio of CD169^{low} and CD169^{high} bone marrow stromal macrophages was similar between the infected and naïve RAG2^{-/-} mice (**Fig. 5G**).

Finally, we reconstituted B6.Rag2^{-/-} mice by adoptive transfer of CD4⁺ T cells prior to infection with *L. donovani*. B6.Rag2^{-/-} mice receiving CD4⁺ T cells displayed anemia similar to wild type immunocompetent mice, as measured by both erythrocyte count and hematocrit (**Fig. 5H and I**). In contrast to these results obtained using adoptively transferred wild type CD4⁺ T cells, CD4⁺ T cells isolated from IFN γ -deficient B6.Ifng^{-/-} mice we unable to induce anemia (**Fig. 5H and I**), despite equally efficient engraftment and activation (**S6 Figure**). As expected, IFN γ KO T cells were defective compared to wild type CD4⁺ T cells in terms of controlling systemic parasite load (**S7 Figure**). Collectively, these data support the conclusion that both the medullary changes in erythropoiesis and peripheral anemia seen in experimental VL arise as a consequence of CD4⁺ T cell activation and IFN γ production, independently of any potential contributions from splenomegaly.

Discussion

Although evidence abounds that VL causes hematological alterations in humans, dogs and experimental model such as hamsters, very little is known about the underlying mechanisms. In the present study, we show using an experimental murine model that CD4⁺ T cell-dependent adaptive immune responses to *L. donovani* underpin anemia through a pathway that involves repressed BM erythropoiesis consequent on alterations in the stromal microenvironment of the erythropoietic niche.

We show here that C57BL/6 mice chronically infected with *L. donovani* presented with a bicytopenia characterized by normocytic anemia and thrombocytopenia. These findings are consistent with the hematological data typically reported in human studies of VL, though indicate that in this strain of mice at least, there is no accompanying leucopenia. Anemia is often complex and multifactorial and it is likely that different models of disease may to a greater or lesser extent exemplify different underlying mechanisms. For example, multiple mechanisms have been proposed based on clinical observations for the profound anemia observed in human VL, including immune-mediated hemolysis [32] or splenic sequestration [10, 32, 33]. In hamsters infected with *L. donovani*, anemia associated with lethal infection was correlated with increased apoptosis of erythroid progenitors and an increase of IFN γ in the BM and spleen [21]. Our data in murine VL indicates that the spleen may have counteracting roles, on the one hand permitting enhanced erythrophagocytosis [21], but on the other serving as a site of extramedullary compensatory erythropoiesis. Indeed, it is likely that these events may balance each other, resulting in a mild anemia in intact mice that is subsequently unaltered by splenectomy. The fact that a mild anemia is present in infected mice independent of the presence or absence of a spleen, with dysplastic erythroid features, provides a convenient tool to allow exploration of pathological mechanisms operating within the BM microenvironment. Although we also observe thrombocytopenia in *L. donovani*-infected mice, the mechanisms regulating this process appear distinct from that controlling erythropoiesis and will be reported elsewhere.

Our analysis of the BM microenvironment that supports erythropoiesis has for the first time demonstrated that anemia in murine models of VL represents an aspect of CD4⁺ T cell mediated immunopathology. BM resident stromal macrophages, identified by the expression

of the sialoadhesin CD169 [34], were reduced in number in infected mice. CD169⁺ stromal macrophages have been shown to be essential for stress erythropoiesis e.g. following chemically-induced anemia, but their depletion causes minimal disruption of physiological erythropoiesis. In these studies, there was no correlation between overt anemia and a reduction of erythroid progenitors in the BM [7]. These data are in line with our observations, since in our model of EVL, chronic infection results only in a mild anemia despite a dramatic reduction of erythroid progenitors in the bone marrow as observed in myelogram and flow cytometry analysis. We have previously shown that *L.donovani* amastigotes readily parasitize CD169⁺ BM stromal macrophages during chronic infection and that infection of these cells directly supports an increase in their capacity to support myelopoiesis [26]. Our current data extends these observations by indicating that the reduction of the number of CD169⁺ stromal macrophages is not a direct consequence of parasitism, as infected B6.*Rag2*^{-/-} mice have significantly increased parasite loads in the BM, yet show no changes in stromal macrophage number. Rather, our data suggest that loss of stromal macrophages is a further consequence of T cell dependent immune responses.

While CD169⁺ stromal macrophages were reduced in number, the total number of BM macrophages remained stable or increased during infection. It is unclear if loss of CD169⁺ stromal macrophages represents depletion or conversion to a different phenotype, for which specific lineage tracking studies would be required. STING-mediated activation of BM CD169⁺ macrophages has been shown to be essential to type I IFN production by plasmacytoid dendritic in a malaria mouse model [35], indicating that these cells are directly sensitive to infections. Similarly, dexamethasone treatment induces CD169 expression on the surface of human macrophages, promoting in the same time their erythropoiesis-supporting function [36]. Hence, the a stromal “CD169” phenotype can be acquired in differentiated

macrophages and is responsive to inflammatory signals. Interestingly, dexamethasone is also an inhibitor of iNOS [37], thus suggesting a role for NO in EVL-induced anemia. Previously, CD169⁺ macrophages have been shown to be depleted by G-CSF administration [38]. We have observed a consistent upregulation of circulating G-CSF in infected mice (data not shown) but to date our attempts to convincingly neutralize G-CSF in vivo have been unsuccessful. Hence, direct evidence is still needed to support a role for G-CSF in VL-induced anemia.

In hamsters and mice, infection with *L. donovani* causes an increase of erythroid burst forming units (BFU-E) from the bone marrow in colony formation assays [22, 25]. These represent very early progenitors of erythroid cells, prior to the pro-erythroblast stage. In the current study, we show by flow cytometry that only later stages of erythroid differentiation, at or after the pro-erythroblast stage, are affected by infection. This is also reflected in differential counts of bone marrow cells, showing that nucleated mature erythroid cells were reduced in infected mice. Furthermore, conditional depletion of CD169⁺ cells in a mouse model did not alter the BFU-E content in the BM of mice [7]. These data are collectively consistent with macrophage-dependent erythroblastic islands functioning to support erythropoiesis from the erythroblast stage onwards.

We also report that CXCL12-producing mesenchymal stromal cells are affected during VL. Infection led to a reduction of *Cxcl12* mRNA accumulation in the bone marrow, correlating with a reduction in the number of CXCL12-expressing cells. The main mechanism of G-CSF-induced down-regulation of CXCL12 is protease-dependent [39] but a more complex model including transcriptional regulation has also been reported. While down-regulation of CXCL12 is a potentially due to up-regulation of G-CSF, CD169 macrophages are also

responsible for the retention of CAR cells in the bone marrow. It is likely that these mechanisms together factor into the loss of stromal support in the BM. In the case of *E. coli* infection, heightened levels of G-CSF led to a reduction in CXCL12 expression in the BM via Toll-like receptor and NOD1/2 signaling [3]. This study did not however directly enumerate CXCL12-producing cells in BM, our observations here being the first reported instance of loss of these cells during infectious disease.

In summary, we have shown that IFN γ -producing CD4⁺ T cells contribute to anemia in a model of VL, via a mechanism that involves loss of both macrophages and mesenchymal stromal elements from the BM erythropoietic niche leading to dyserythropoiesis. Whether these effects are the result of direct IFN γ signaling on CD169⁺ macrophages and / or mesenchymal stromal cells, whether they reflect indirect effects of IFN γ on third party cells or whether they are the consequence of induced expression of one of the many IFN-responsive genes remains to be determined. We have also recently shown that CD4⁺ T cells producing both IFN γ and TNF accumulate in large numbers in the BM of infected mice, via a mechanism requiring CD4⁺ T cell-intrinsic TNF receptor signaling. These cells drive functional exhaustion within the long-term HSC compartment [28]. Collectively, therefore, a picture emerges whereby CD4⁺ T cells play a pathogenic role in the BM that leads to BM failure with both short and long-term consequences for hematological health. These data provide an imperative for similar studies in humans, to determine whether CD4⁺ T cells likewise have a causative role in the hematological changes associated with VL or indeed other infections where BM accumulation of activated effector T cells occurs.

Acknowledgements

443 The authors thank the staff of the Biological Services Facility for animal husbandry and the
444 staff of the BioSciences Technology Facility Imaging and Cytometry Laboratory for
445 assistance with flow and confocal analysis.

446 **References**

- 447 1. Sugiyama T, Kohara H, Noda M, Nagasawa T. Maintenance of the hematopoietic
448 stem cell pool by CXCL12-CXCR4 chemokine signaling in bone marrow stromal cell niches.
449 *Immunity*. 2006;25(6):977-88. Epub 2006/12/19. doi: 10.1016/j.immuni.2006.10.016.
450 PubMed PMID: 17174120.
- 451 2. Pietras EM. Inflammation: a key regulator of hematopoietic stem cell fate in health
452 and disease. *Blood*. 2017;130(15):1693-8. Epub 2017/09/07. doi: 10.1182/blood-2017-06-
453 780882. PubMed PMID: 28874349; PubMed Central PMCID: PMC5639485.
- 454 3. Burberry A, Zeng MY, Ding L, Wicks I, Inohara N, Morrison SJ, et al. Infection
455 mobilizes hematopoietic stem cells through cooperative NOD-like receptor and Toll-like
456 receptor signaling. *Cell Host Microbe*. 2014;15(6):779-91. Epub 2014/06/03. doi:
457 10.1016/j.chom.2014.05.004. PubMed PMID: 24882704; PubMed Central PMCID:
458 PMC4085166.
- 459 4. Johns JL, Borjesson DL. Downregulation of CXCL12 signaling and altered
460 hematopoietic stem and progenitor cell trafficking in a murine model of acute *Anaplasma*
461 phagocytophilum infection. *Innate Immun*. 2012;18(3):418-28. Epub 2011/10/04. doi:
462 10.1177/1753425911413794. PubMed PMID: 21964802; PubMed Central PMCID:
463 PMC3905609.
- 464 5. Musaya J, Matovu E, Nyirenda M, Chisi J. Role of cytokines in *Trypanosoma brucei*-
465 induced anaemia: A review of the literature. *Malawi Med J*. 2015;27(2):45-50. Epub
466 2015/09/26. PubMed PMID: 26405511; PubMed Central PMCID: PMC4562079.
- 467 6. Ghosh K, Ghosh K. Pathogenesis of anemia in malaria: a concise review. *Parasitol*
468 *Res*. 2007;101(6):1463-9. Epub 2007/09/18. doi: 10.1007/s00436-007-0742-1. PubMed
469 PMID: 17874326.
- 470 7. Chow A, Huggins M, Ahmed J, Hashimoto D, Lucas D, Kunisaki Y, et al. CD169(+)
471 macrophages provide a niche promoting erythropoiesis under homeostasis and stress. *Nat*
472 *Med*. 2013;19(4):429-36. Epub 2013/03/19. doi: 10.1038/nm.3057. PubMed PMID:
473 23502962; PubMed Central PMCID: PMC3983996.
- 474 8. Casanova-Acebes M, Pitaval C, Weiss LA, Nombela-Arrieta C, Chevre R, N AG, et
475 al. Rhythmic modulation of the hematopoietic niche through neutrophil clearance. *Cell*.
476 2013;153(5):1025-35. Epub 2013/05/28. doi: 10.1016/j.cell.2013.04.040. PubMed PMID:
477 23706740; PubMed Central PMCID: PMC4128329.
- 478 9. Chow A, Lucas D, Hidalgo A, Mendez-Ferrer S, Hashimoto D, Scheiermann C, et al.
479 Bone marrow CD169+ macrophages promote the retention of hematopoietic stem and
480 progenitor cells in the mesenchymal stem cell niche. *J Exp Med*. 2011;208(2):261-71. Epub
481 2011/02/02. doi: 10.1084/jem.20101688. PubMed PMID: 21282381; PubMed Central
482 PMCID: PMC3039855.
- 483 10. Cartwright GE, Chung HL, Chang A. Studies on the pancytopenia of kala-azar.
484 *Blood*. 1948;3(3):249-75. Epub 1948/03/01. PubMed PMID: 18902574.
- 485 11. Goto Y, Cheng J, Omachi S, Morimoto A. Prevalence, severity, and pathogenesis of
486 anemia in visceral leishmaniasis. *Parasitol Res*. 2017;116(2):457-64. Epub 2016/11/09. doi:
487 10.1007/s00436-016-5313-x. PubMed PMID: 27822583.
- 488 12. Belo VS, Struchiner CJ, Barbosa DS, Nascimento BW, Horta MA, da Silva ES, et al.
489 Risk factors for adverse prognosis and death in American visceral leishmaniasis: a meta-

analysis. PLoS Negl Trop Dis. 2014;8(7):e2982. Epub 2014/07/25. doi: 10.1371/journal.pntd.0002982. PubMed PMID: 25058582; PubMed Central PMCID: PMC4109848.

13. Coura-Vital W, Araujo VE, Reis IA, Amancio FF, Reis AB, Carneiro M. Prognostic factors and scoring system for death from visceral leishmaniasis: an historical cohort study in Brazil. PLoS Negl Trop Dis. 2014;8(12):e3374. Epub 2014/12/17. doi: 10.1371/journal.pntd.0003374. PubMed PMID: 25503575; PubMed Central PMCID: PMC4263605.

14. Alexandropoulou O, Tsolia M, Kossiva L, Giannaki M, Karavanaki K. Visceral leishmaniasis: a common cause of post-infectious febrile pancytopenia in children in an endemic area: experience of a children's tertiary hospital. Pediatr Emerg Care. 2012;28(6):533-7. Epub 2012/06/02. doi: 10.1097/PEC.0b013e3182587d5d. PubMed PMID: 22653455.

15. Besada E, Njalla RJ, Nossent JC. Imported case of visceral leishmaniasis presenting as pancytopenia in a Norwegian patient treated with methotrexate and etanercept for psoriasis arthritis. Rheumatol Int. 2013;33(10):2687-9. Epub 2012/08/14. doi: 10.1007/s00296-012-2483-4. PubMed PMID: 22886470.

16. Koster KL, Laws HJ, Troeger A, Meisel R, Borkhardt A, Oommen PT. Visceral Leishmaniasis as a Possible Reason for Pancytopenia. Front Pediatr. 2015;3:59. Epub 2015/07/16. doi: 10.3389/fped.2015.00059. PubMed PMID: 26176005; PubMed Central PMCID: PMC4483513.

17. Kopterides P, Halikias S, Tsavaris N. Visceral leishmaniasis masquerading as myelodysplasia. Am J Hematol. 2003;74(3):198-9. Epub 2003/10/31. doi: 10.1002/ajh.10408. PubMed PMID: 14587050.

18. Yarali N, Fisgin T, Duru F, Kara A. Myelodysplastic features in visceral leishmaniasis. Am J Hematol. 2002;71(3):191-5. Epub 2002/11/01. doi: 10.1002/ajh.10200. PubMed PMID: 12410574.

19. Samanta S, Ghoshal A, Bhattacharya K, Saha B, Walden P, Mandal C. Sialoglycosylation of RBC in visceral leishmaniasis leads to enhanced oxidative stress, calpain-induced fragmentation of spectrin and hemolysis. PLoS One. 2012;7(7):e42361. Epub 2012/08/04. doi: 10.1371/journal.pone.0042361. PubMed PMID: 22860118; PubMed Central PMCID: PMC409180.

20. Saha Roy S, Chowdhury KD, Sen G, Biswas T. Oxidation of hemoglobin and redistribution of band 3 promote erythrophagocytosis in visceral leishmaniasis. Mol Cell Biochem. 2009;321(1-2):53-63. Epub 2008/09/09. doi: 10.1007/s11010-008-9909-z. PubMed PMID: 18777164.

21. Morimoto A, Omachi S, Osada Y, Chambers JK, Uchida K, Sanjoba C, et al. Hemophagocytosis in Experimental Visceral Leishmaniasis by *Leishmania donovani*. PLoS Negl Trop Dis. 2016;10(3):e0004505. Epub 2016/03/05. doi: 10.1371/journal.pntd.0004505. PubMed PMID: 26942577; PubMed Central PMCID: PMC4778860.

22. Lafuse WP, Story R, Mahylis J, Gupta G, Varikuti S, Steinkamp H, et al. *Leishmania donovani* infection induces anemia in hamsters by differentially altering erythropoiesis in bone marrow and spleen. PLoS One. 2013;8(3):e59509. Epub 2013/03/28. doi: 10.1371/journal.pone.0059509. PubMed PMID: 23533629; PubMed Central PMCID: PMC3606219.

23. Bankoti R, Stager S. Differential Regulation of the Immune Response in the Spleen and Liver of Mice Infected with *Leishmania donovani*. *J Trop Med*. 2012;2012:639304. Epub 2011/08/04. doi: 10.1155/2012/639304. PubMed PMID: 21811511; PubMed Central PMCID: PMC3143424.
24. Engwerda CR, Ato M, Kaye PM. Macrophages, pathology and parasite persistence in experimental visceral leishmaniasis. *Trends Parasitol*. 2004;20(11):524-30. Epub 2004/10/09. doi: 10.1016/j.pt.2004.08.009. PubMed PMID: 15471704.
25. Cotterell SE, Engwerda CR, Kaye PM. Enhanced hematopoietic activity accompanies parasite expansion in the spleen and bone marrow of mice infected with *Leishmania donovani*. *Infect Immun*. 2000;68(4):1840-8. Epub 2000/03/18. PubMed PMID: 10722572; PubMed Central PMCID: PMC397356.
26. Cotterell SE, Engwerda CR, Kaye PM. *Leishmania donovani* infection of bone marrow stromal macrophages selectively enhances myelopoiesis, by a mechanism involving GM-CSF and TNF-alpha. *Blood*. 2000;95(5):1642-51. Epub 2000/02/26. PubMed PMID: 10688819.
27. Abidin BM, Hammami A, Stager S, Heinonen KM. Infection-adapted emergency hematopoiesis promotes visceral leishmaniasis. *PLoS Pathog*. 2017;13(8):e1006422. Epub 2017/08/09. doi: 10.1371/journal.ppat.1006422. PubMed PMID: 28787450; PubMed Central PMCID: PMC5560750.
28. Pinto AI, Brown N, Preham O, Doehl JSP, Ashwin H, Kaye PM. TNF signalling drives expansion of bone marrow CD4+ T cells responsible for HSC exhaustion in experimental visceral leishmaniasis. *PLoS Pathog*. 2017;13(7):e1006465. Epub 2017/07/04. doi: 10.1371/journal.ppat.1006465. PubMed PMID: 28671989; PubMed Central PMCID: PMC5510901.
29. Koulis M, Pop R, Porpiglia E, Shearstone JR, Hidalgo D, Socolovsky M. Identification and analysis of mouse erythroid progenitors using the CD71/TER119 flow-cytometric assay. *J Vis Exp*. 2011;(54). Epub 2011/08/19. doi: 10.3791/2809. PubMed PMID: 21847081; PubMed Central PMCID: PMC3211121.
30. Omatsu Y, Sugiyama T, Kohara H, Kondoh G, Fujii N, Kohno K, et al. The essential functions of adipo-osteogenic progenitors as the hematopoietic stem and progenitor cell niche. *Immunity*. 2010;33(3):387-99. Epub 2010/09/21. doi: 10.1016/j.immuni.2010.08.017. PubMed PMID: 20850355.
31. Frenette PS, Pinho S, Lucas D, Scheiermann C. Mesenchymal stem cell: keystone of the hematopoietic stem cell niche and a stepping-stone for regenerative medicine. *Annu Rev Immunol*. 2013;31:285-316. Epub 2013/01/10. doi: 10.1146/annurev-immunol-032712-095919. PubMed PMID: 23298209.
32. Woodruff AW, Topley E, Knight R, Downie CG. The anaemia of kala-azar. *Br J Haematol*. 1972;22(3):319-29. Epub 1972/03/01. PubMed PMID: 4552217.
33. Varma N, Naseem S. Hematologic changes in visceral leishmaniasis/kala azar. *Indian J Hematol Blood Transfus*. 2010;26(3):78-82. Epub 2011/09/03. doi: 10.1007/s12288-010-0027-1. PubMed PMID: 21886387; PubMed Central PMCID: PMC3002089.
34. Crocker PR, Gordon S. Mouse macrophage hemagglutinin (sheep erythrocyte receptor) with specificity for sialylated glycoconjugates characterized by a monoclonal antibody. *J Exp Med*. 1989;169(4):1333-46. Epub 1989/04/01. PubMed PMID: 2926328; PubMed Central PMCID: PMC2189241.

35. Spaulding E, Fooksman D, Moore JM, Saidi A, Feintuch CM, Reizis B, et al. STING-Licensed Macrophages Prime Type I IFN Production by Plasmacytoid Dendritic Cells in the Bone Marrow during Severe *Plasmodium yoelii* Malaria. *PLoS Pathog.* 2016;12(10):e1005975. Epub 2016/10/30. doi: 10.1371/journal.ppat.1005975. PubMed PMID: 27792766; PubMed Central PMCID: PMC5085251.
36. Heideveld E, Hampton-O'Neil LA, Cross SJ, van Alphen FPJ, van den Biggelaar M, Toye AM, et al. Glucocorticoids induce differentiation of monocytes towards macrophages that share functional and phenotypical aspects with erythroblastic island macrophages. *Haematologica.* 2017. Epub 2017/12/30. doi: 10.3324/haematol.2017.179341. PubMed PMID: 29284682.
37. Soderberg M, Raffalli-Mathieu F, Lang MA. Regulation of the murine inducible nitric oxide synthase gene by dexamethasone involves a heterogeneous nuclear ribonucleoprotein I (hnRNPI) dependent pathway. *Mol Immunol.* 2007;44(12):3204-10. Epub 2007/03/24. doi: 10.1016/j.molimm.2007.01.029. PubMed PMID: 17379310.
38. Jacobsen RN, Forristal CE, Raggatt LJ, Nowlan B, Barbier V, Kaur S, et al. Mobilization with granulocyte colony-stimulating factor blocks medullar erythropoiesis by depleting F4/80(+)VCAM1(+)CD169(+)ER-HR3(+)Ly6G(+) erythroid island macrophages in the mouse. *Exp Hematol.* 2014;42(7):547-61 e4. Epub 2014/04/12. doi: 10.1016/j.exphem.2014.03.009. PubMed PMID: 24721610.
39. Levesque JP, Liu F, Simmons PJ, Betsuyaku T, Senior RM, Pham C, et al. Characterization of hematopoietic progenitor mobilization in protease-deficient mice. *Blood.* 2004;104(1):65-72. Epub 2004/03/11. doi: 10.1182/blood-2003-05-1589. PubMed PMID: 15010367.
40. Yang M, Busche G, Ganser A, Li Z. Morphology and quantitative composition of hematopoietic cells in murine bone marrow and spleen of healthy subjects. *Ann Hematol.* 2013;92(5):587-94. Epub 2013/01/12. doi: 10.1007/s00277-012-1653-5. PubMed PMID: 23307597.

Figure Legends.

Fig. 1. *L. donovani* infection induces extramedullary erythropoiesis in the spleen.

A and B. Gating strategy for identification of pro-erythroblasts ($CD45^-CD71^{high}TER119^{low}$) and erythroblasts ($CD45^-CD71^{high/low}TER119^{high}$) in the spleens of naïve (A) and infected (B) mice. Plots are gated on $CD45^-$ live cells and equal number of live cells. **C.** Frequency of pro-erythroblasts in the spleen. **D.** Frequency of erythroblasts in the spleen. **E.** Absolute number of pro-erythroblasts per spleen. **F.** Absolute number of erythroblasts per spleen. Absolute numbers were calculated by multiplying the cell frequencies by the total numbers of cells per spleen. **G and H.** Representative histology of spleens from control (G) and infected (H) mice. Sections were stained for F4/80 (green), TER119 (white) CD71 (red) and counterstained with DAPI (Blue). F4/80 demarcates the red pulp. All mice were infected for 28 days. Data represent mean \pm SEM (unpaired t-test with Welch's correction; n=8 mice per group from two independent experiments).

Fig. 2. Medullary erythropoiesis is repressed during experimental visceral leishmaniasis

A. Femurs isolated from *L. donovani*-infected mice and age-matched naïve mice. Representative from 30 mice per group from 10 independent experiment. **B.** Hematocrit in naïve and infected mice with and without splenectomy (Sp_x). **C and D.** Confocal imaging of 5 μ m-thick femoral sections from naïve (C) and infected (D) mice stained with DAPI (blue) and TER119 (white). Representative of 6 mice per group from 2 independent experiments. **E.** Representative flow cytometry analysis of $CD45^-$ BM cells from infected mouse using the erythroid surface markers CD71 (transferrin receptor) and TER-119. Pro-erythroblasts are $CD45^-CD71^+TER119^{low}$ and erythroblasts are $CD45^-CD71^{+/+}TER119^{high}$. **F.** Absolute number of pro-erythroblasts per femur + tibia in sham operated and Sp_x mice. Mann Whitney test; n=14 mice per group from 4

independent experiments. Data represent mean \pm SEM. All experiments were performed 28 days post-infection.

Fig. 3. Infection with *L. donovani* reduces the number of CD169⁺ stromal macrophages in BM.

A. BM stromal macrophages were identified as Gr-1⁻ CD115⁻ F4/80⁺ SSC^{low} cells [9]. **B.** CD169 expression on BM macrophages of naïve (green) and infected (red) mice. Isotype control (blue) is representative of both naïve and infected mice. **C.** Absolute number of macrophages per leg (1 femur + 1 tibia) according to the gating described in A and B. **D.** Absolute number of CD169^{low} and CD169^{high} stromal macrophages based on gating in B. Absolute numbers were calculated from the frequencies multiplied by the total bone marrow cells isolated from each mouse. Data represent mean \pm SEM. All experiments were performed 28 days after infection. (unpaired t-test; n=10 mice per group from 2 independent experiments)

Fig. 4. *L. donovani* infection causes a reduction in CXCL-12-expressing cells in the BM.

A. *Cxcl12* mRNA accumulation in BM of naïve and infected mice, determined by qRT-PCR. **B.** Visualisation of CXCL12-expressing cells using naïve and infected *Cxcl12*-DsRed reporter mice. Sectioned were co-stained for laminin (green) and counterstained with DAPI (blue). **C and D.** Flow cytometry analysis of DsRed⁺ cells in naïve (C) and infected (D) *Cxcl12*-DsRed reporter mice. Dot plots show identical number of cells, gated on live single cells. **E.** Frequency of DsRed⁺ cells. **F.** Absolute number of DsRed⁺ cells per femur, calculated from the frequency of DsRed⁺ cells in (E) multiplied by the total bone marrow cell count (Mann Whitney test; Data from 5 naïve mice and 9 infected mice from 2 independent experiments). **G.** Number of CFU-F per million BM cells (Unpaired t-test; n=7 mice per group from 2 independent experiments). Data represent mean \pm SEM. All experiments were performed 28 days post-infection with *L. donovani*.

Fig. 5 IFN γ -producing CD4⁺ T cells mediate repression of medullary erythropoiesis in experimental VL.

A. Frequency of leucocyte subsets accumulating in the BM of sham-operated or Sp_x naïve (open bars) and infected (black bars) mice. Data from one experiment (n=5 mice per group; Mann-Whitney: not significant (ns)). **B.** T cell accumulation in BM visualized using hCD2-DsRed mice. Sectioned were counterstained with DAPI (blue). Femurs representative of 15 mice per group examined from 3 independent experiments. **C and D.** Absolute numbers of pro-erythroblasts (C) and erythroblasts (D) in the BM of naïve and infected wild type C57BL/6 or B6.*Rag2*^{-/-} mice. Absolute numbers were calculated by multiplying frequencies by the total BM cell counts (One-way ANOVA with Turkey's multiple comparison test; n=10 mice per group from 2 independent experiments). Data represent mean \pm SEM. **E.** *Cxcl12* mRNA accumulation in total BM cells from naïve and infected B6.*Rag2*^{-/-} mice. Intra-sample standardization was performed by normalization to HPRT and inter-sample standardization was done by normalization to the average expression of the naïve group (n=8 wild-type mice per group, 5 naïve and 7 infected from one experiment). **F.** CD169 expression on BM macrophages of naïve (green) and infected (red) B6.*Rag2*^{-/-} mice. Isotype control (blue) is representative of both naïve and infected mice. **G.** Absolute numbers of macrophages per leg (1 femur + 1 tibia), calculated from the frequencies multiplied by the total bone marrow cells isolated from each mouse (n=3 naïve and 4 infected mice from one experiment). **H and I.** Anemia, measured as RBC count (H) or hematocrit (I) in B6.*Rag2*^{-/-} mice receiving adoptive transfer of either IFN γ -sufficient (WT) or IFN γ -deficient (IFN γ KO) CD4⁺ T cells. (n=4/5 per group; One-way Anova followed by Tukey's multiple comparisons test: not significant (ns), *p \leq 0.05).

Table 1. Hematological characteristics of C57BL/6 mice infected for 28 days with *L. donovani*.

	<i>Naive</i>	<i>Infected</i>
<i>WBC</i> ($\times 10^3/\text{ul}$)	6.803 \pm 0.864	5.758 \pm 0.659
<i>NE</i> ($\times 10^3/\text{ul}$)	1.671 \pm 0.309	1.108 \pm 0.128
<i>LY</i> ($\times 10^3/\text{ul}$)	4.486 \pm 0.455	4.072 \pm 0.626
<i>MO</i> ($\times 10^3/\text{ul}$)	0.296 \pm 0.072	0.230 \pm 0.017
<i>EO</i> ($\times 10^3/\text{ul}$)	0.259 \pm 0.077	0.108 \pm 0.058
<i>BA</i> ($\times 10^3/\text{ul}$)	0.077 \pm 0.026	0.013 \pm 0.003
<i>RBC</i> ($\times 10^6/\text{ul}$)	8.110 \pm 0.143	6.572 \pm 0.241***
<i>HB</i> (g/dl)	9.593 \pm 0.213	8.169 \pm 0.219***
<i>HCT</i> (%)	41.860 \pm 0.900	34.020 \pm 1.091***
<i>MCV</i> (fl)	51.610 \pm 0.577	51.990 \pm 1.035
<i>MCH</i> (pg)	11.860 \pm 0.227	12.520 \pm 0.198*
<i>MCHC</i> (g/dl)	23.040 \pm 0.663	24.130 \pm 0.509
<i>PLT</i> ($\times 10^3/\text{ul}$)	583.000 \pm 45.680	281.500 \pm 26.39***
<i>MPV</i> (fl)	4.293 \pm 0.143	5.354 \pm 0.084***

Bold values are significant: *p<0.05; *** p<0.0001

Table 2. Comparative myelogram of naïve mice and mice infected with *L. donovani* for 28 days.

	<i>Naive</i>	<i>Infected</i>
<i>Myeloid : Erythroid Ratio</i>	1.5 (1.3-2.0)	2.1 (1.7-2.8)*
<i>Precursor Myeloid : Mature Myeloid</i>	0.02 (0.01-0.03)	0.1 (0.04-0.19)*
<i>Nucleated Erythroid Precursor : Nucleated Erythroid Mature</i>	0.02 (0.01-0.03)	0.03 (0.02-0.05)
<i>Precursor Myeloid Cells (%)</i>	1.0 (0.6-1.1)	4.8 (2.6-6.0)*
<i>Mature Myeloid Cells (%)</i>	39.7 (35.5-42.5)	34.8 (31.0-38.1)*
<i>Nucleated Erythroid Precursor Cells (%)</i>	0.6 (0.4-0.9)	0.6 (0.2-0.9)
<i>Nucleated Erythroid Mature Cells (%)</i>	26.8 (19.4-30.6)	17.8 (11.8-21.1)*
<i>Lymphocytes (%)</i>	33.0 (26.4-37.4)	41.2 (35.7-47.2)*
<i>Plasma cells (%)</i>	0.4 (0.2-0.6)	0.6 (0.2-1.0)
<i>Monocytes (%)</i>	0.0 (0.0-0.2)	0.3 (0.0-0.7)
<i>Macrophages (%)</i>	0.0 (0.0-0.2)	0.0 (0.0-0.1)

Bold values are significant: *p<0.05

Supporting Information Legends

S1 Table. Distribution of infected mice according to normal values of haematological parameters.

S1 Figure Aberrant red cell morphology following *L. donovani* infection

Representative images of M-G Giemsa-stained blood films from naïve (A-D) and d28 *L. donovani*-infected mice (E-H). Red thin arrow: polychromatic red cells; green thin arrow: acanthocytes; yellow thin arrow: schistocytes; black thin arrow: macrocyte; white thin arrow: microcyte; blue thin arrow: elliptocyte; red large arrow: nucleated red blood cell; blue large arrow: lymphocyte; green large arrow: neutrophil.

S2 Figure. Frequency of erythroid precursors in bone marrow.

Frequency of erythroid precursors (pro-erythroblasts and erythroblasts) in the bone marrow of naïve (green) and *L. donovani*-infected (red) B6 mice over time. Precursors were identified on the basis of TER119 and CD71 staining. Unpaired t-test; n=3 mice per group per timepoint).

S3 Figure Myelogram of *L. donovani*-infected BM

BM samples were obtained by aspiration biopsy from iliac crest using 24 G needle attached to a 5mL disposable plastic syringe with 10% EDTA and smears were stained with May-Grünwald Giemsa and analyzed by optical microscopy (Zeiss, Germany) and images using Zen software (Carl Zeiss). A Binucleated erythroid cell. B Megalocyte. C. Atypical mitosis. D Emperipolesis. Examples of such cells are indicated with arrows.

S4 Figure Frequency of T cells in bone marrow

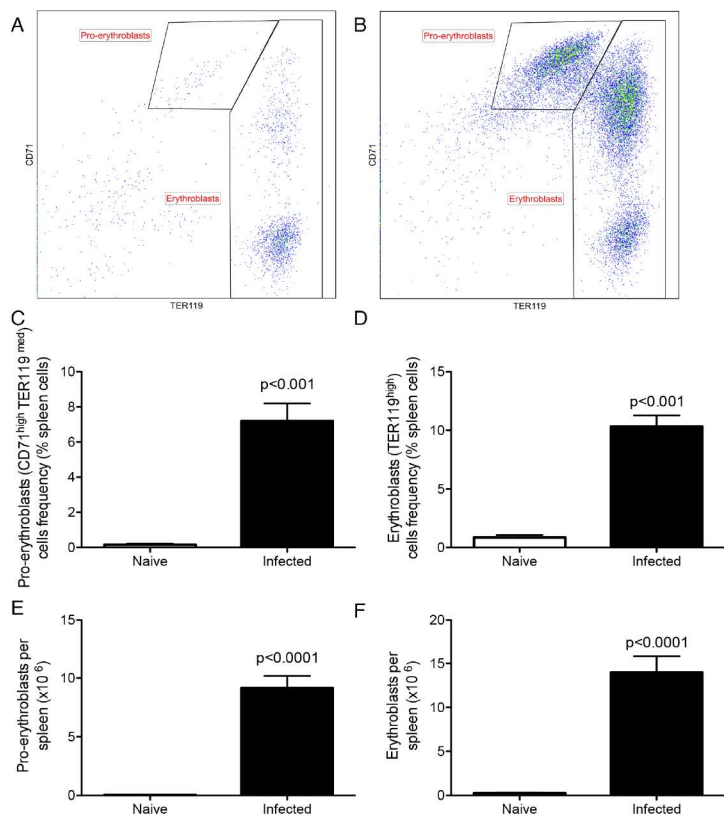
Frequency of CD3⁺ cells in the bone marrow of naïve (green) and *L. donovani*-infected (red) B6 mice over time. Unpaired t-test; n=3 mice per group per timepoint).

S5 Figure. Parasite load in *L. donovani* infected B6 and B6.*Rag2*^{-/-} mice.

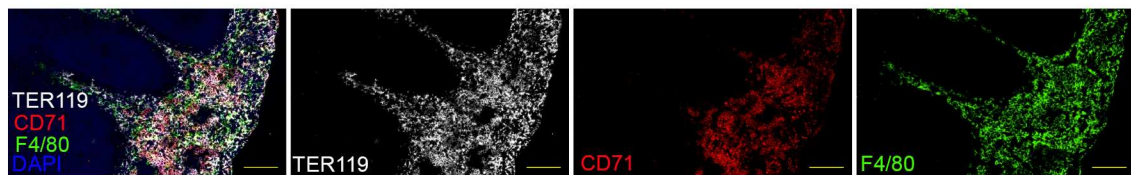
Parasites per 1000 nuclei in the spleen at d28 p.i.. Spleen impressions smears were made on glass slides and stained with Giemsa. Parasites and nuclei were counted microscopically. n=8 wild-type and 6 RAG2^{-/-} mice from 2 independent experiments

S6 Figure. Number and differentiation state of wild type and IFN γ KO CD4⁺ T cells in RAG recipients.

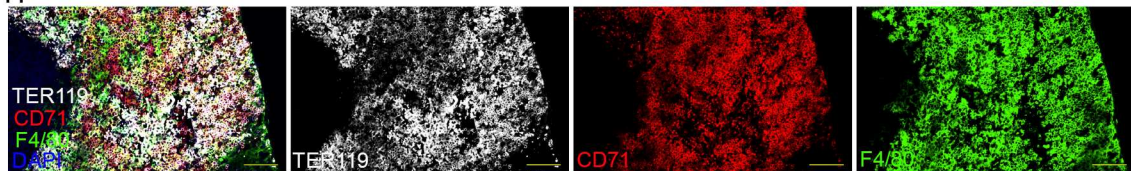
Wild type (black bars) or IFN γ KO (open bars) CD4⁺ T cells were transferred into RAG recipients prior to infection with *L. donovani*. At day 28 p.i., BM CD4⁺ T cells were enumerated and characterized by flow cytometry. **A.** Number of total CD4⁺ T cells and of CD4⁺ T cells with CD44^{hi} and CD44^{lo} phenotype. **B.** Number of CD4⁺ T cells expressing different expression patterns for Ly6C, CD44 and CD127. CD44^{hi}Ly6C^{-/lo}CD127^{-/lo} are often regarded as classical effector cells. Two tibias and femurs were taken per mouse with n=4 mice receiving wild type T cells and n=5 mice receiving KO T cells.

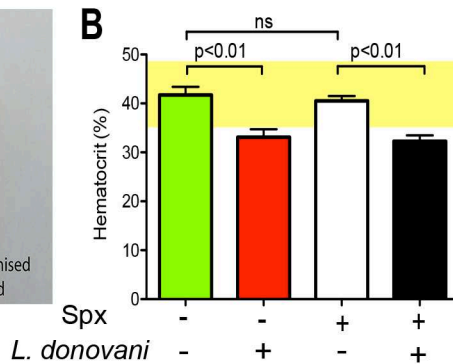
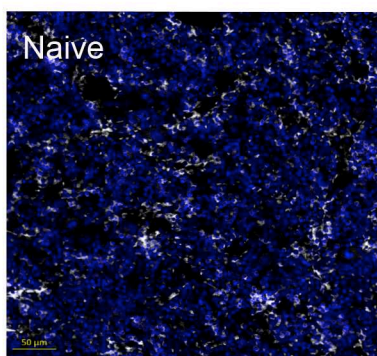
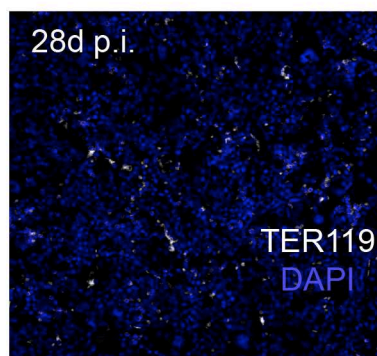
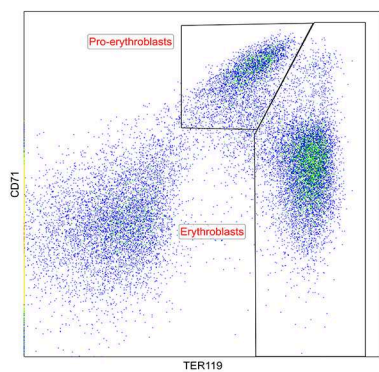
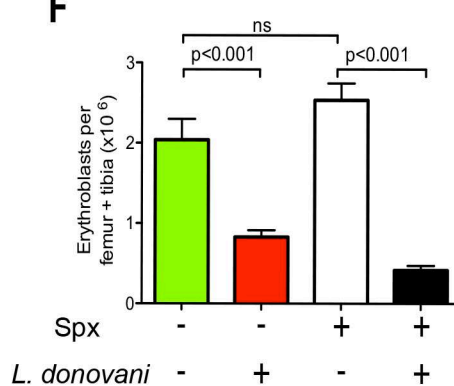


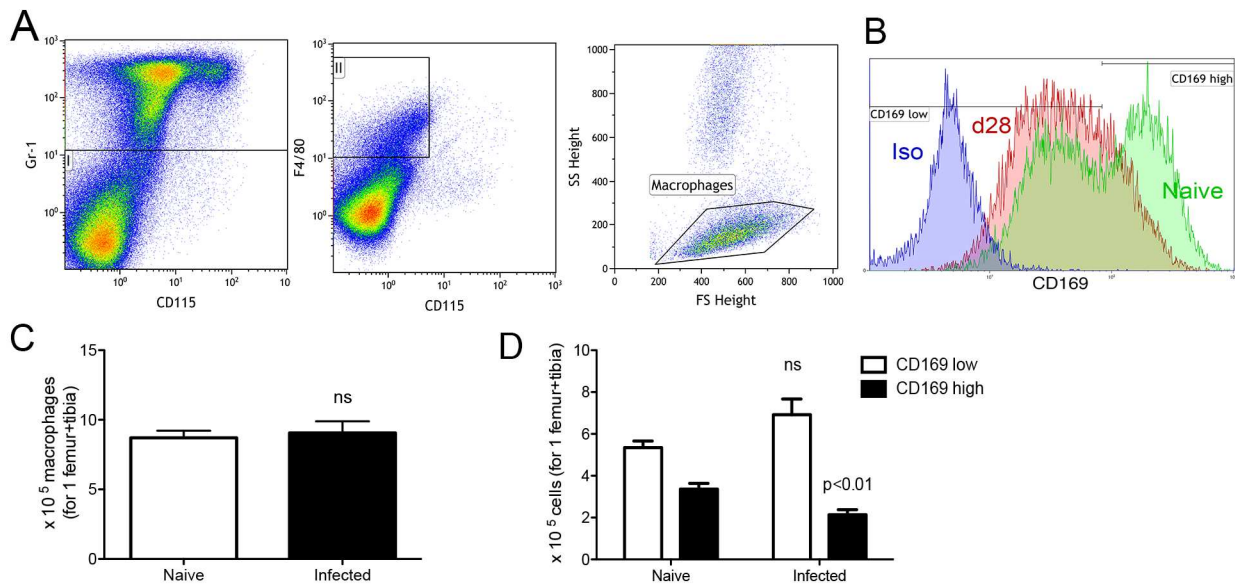
G

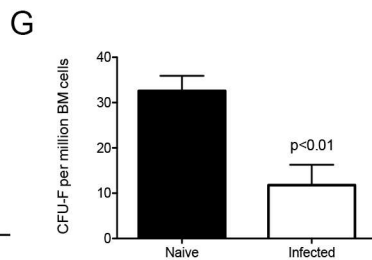
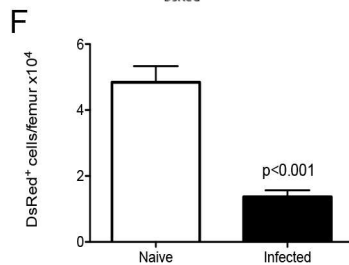
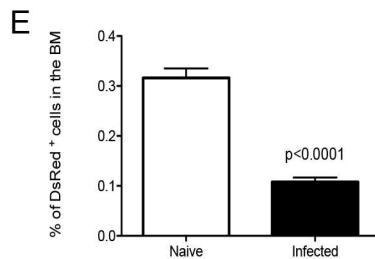
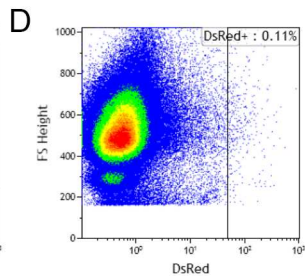
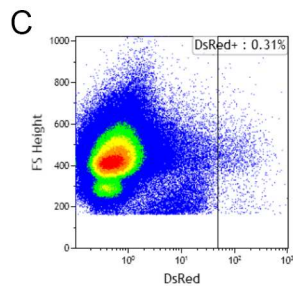
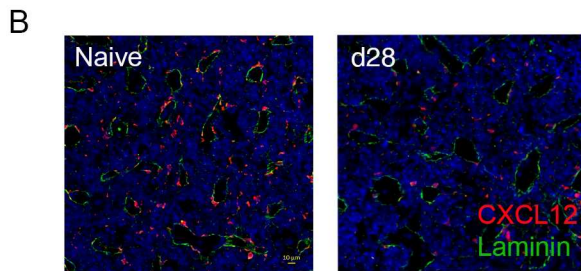
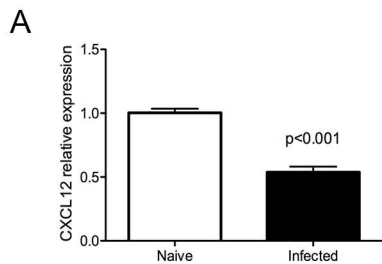


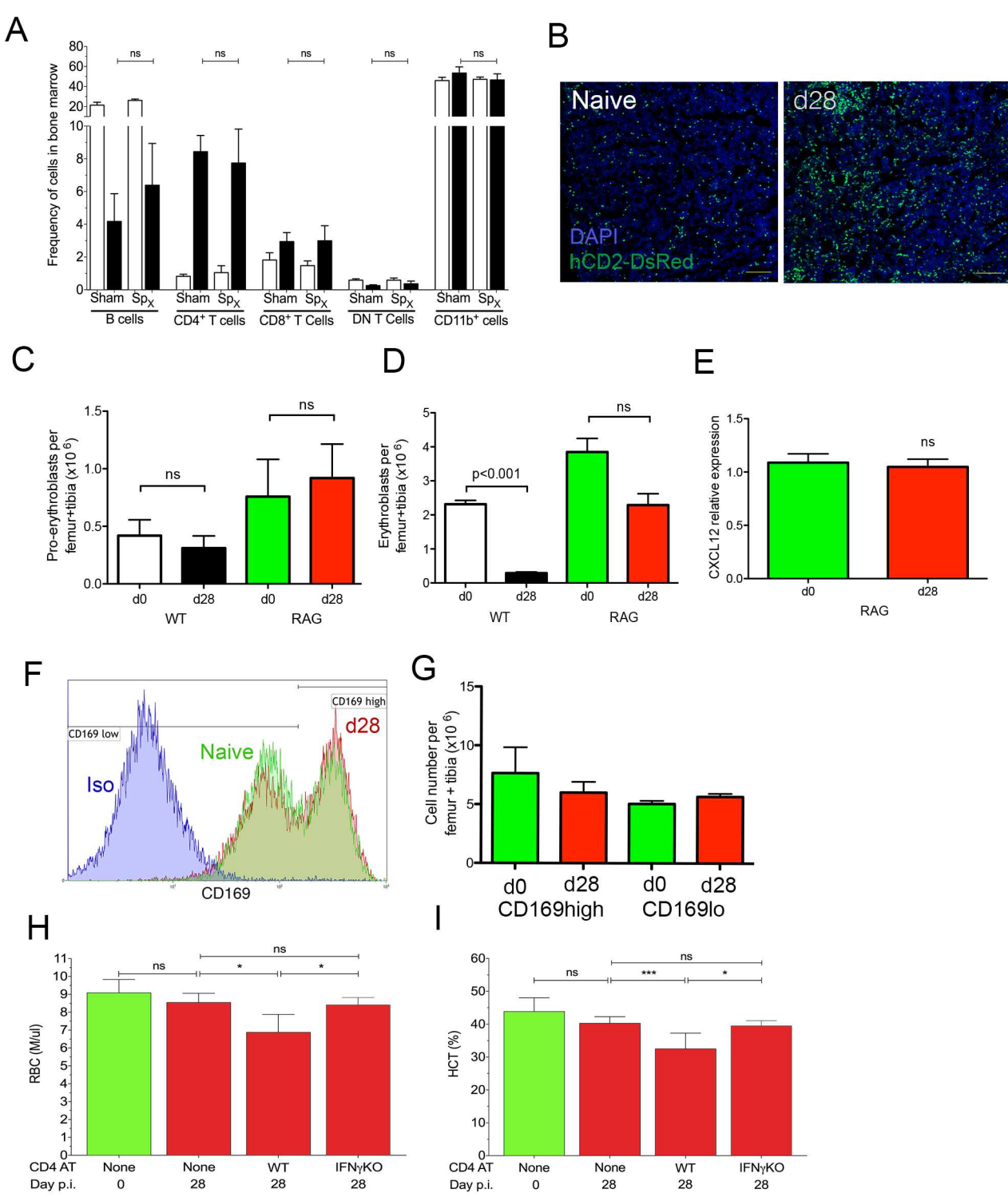
H



A**B****C****D****E****F**





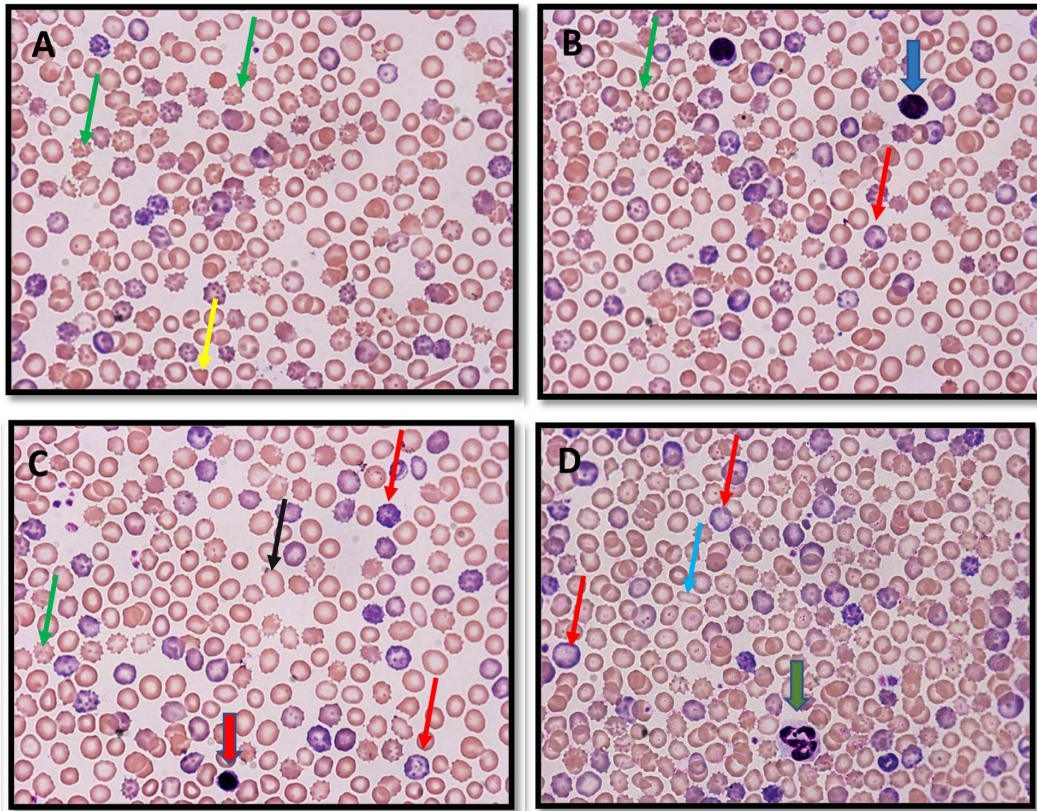


CD4⁺ T cells alter the stromal microenvironment and repress medullary erythropoiesis in murine visceral leishmaniasis. Preham et. al.

S1 Table. Distribution of infected mice according to normal values of haematological parameters.

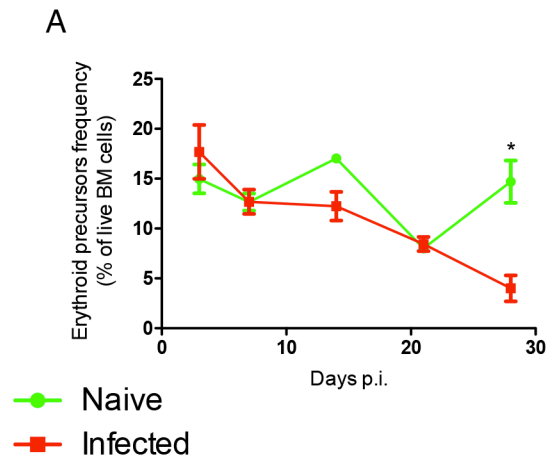
	<i>Reference interval</i>	<i>Distribution relative to reference interval (%)</i>		
		Under	Within	Above
<i>WBC (x10³/ul)</i>	2.40 - 15.73	0	100	0
<i>NE (x10³/ul)</i>	0.37 - 5.03	0	100	0
<i>LY (x10³/ul)</i>	1.96 - 9.01	7.69	92.31	0
<i>MO (x10³/ul)</i>	0.05 - 0.92	0	100	0
<i>EO (x10³/ul)</i>	0.01 - 0.71	0	92.31	7.69
<i>BA (x10³/ul)</i>	0.00 - 0.26	0	100	0
<i>RBC (x10⁶/ul)</i>	7.04 - 9.18	69.23	30.77	0
<i>HB (g/dl)</i>	8.00 - 11.19	30.77	69.23	0
<i>HCT (%)</i>	35.12 - 48.60	61.54	38.46	0
<i>MCV (fl)</i>	47.30 - 55.92	0	76.92	23.08
<i>MCH (pg)</i>	10.16 - 13.56	0	100	0
<i>MCHC (g/dl)</i>	18.08 - 28.00	0	100	0
<i>PLT (x10³/ul)</i>	241.20 - 924.80	38.46	61.54	0
<i>MPV (fl)</i>	3.60 - 5.00	0	23.08	76.92

Supplementary Figures



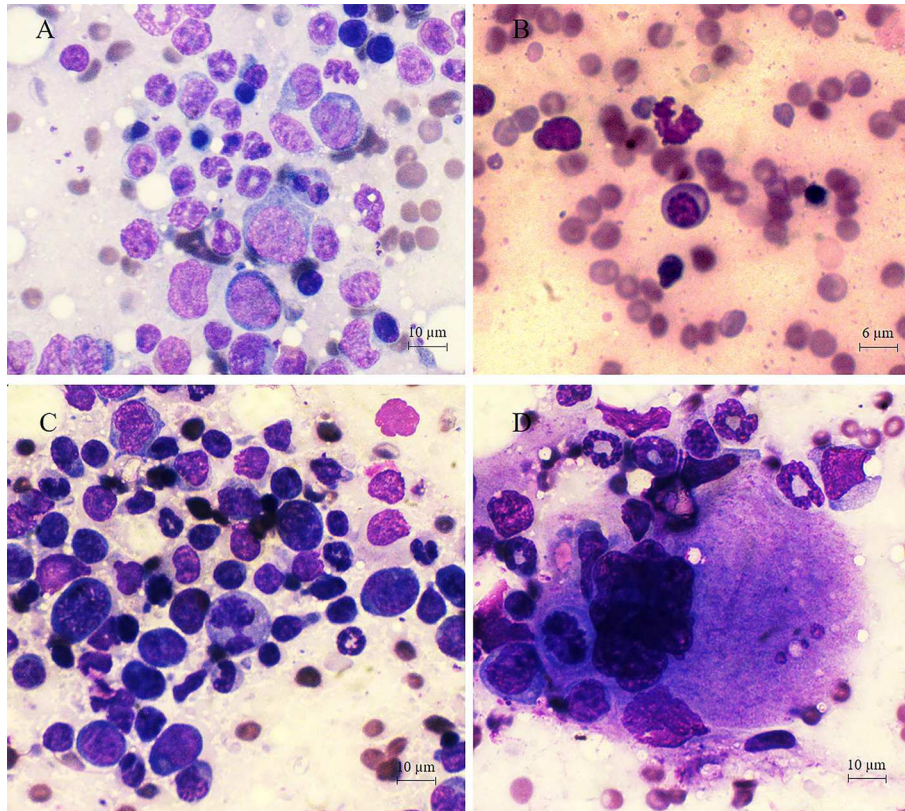
S1 Figure Aberrant red cell morphology following *L. donovani* infection

Representative images of M-G Giemsa-stained blood films from d28 *L. donovani*-infected mice. **A.** green thin arrow: acanthocytes; yellow thin arrow: schistocytes; **B.** red thin arrow: polychromatic red cells; blue large arrow: lymphocyte; **C.** red large arrow: nucleated red blood cell; black thin arrow: macrocyte; **D.** green large arrow: neutrophil. blue thin arrow: elliptocyte



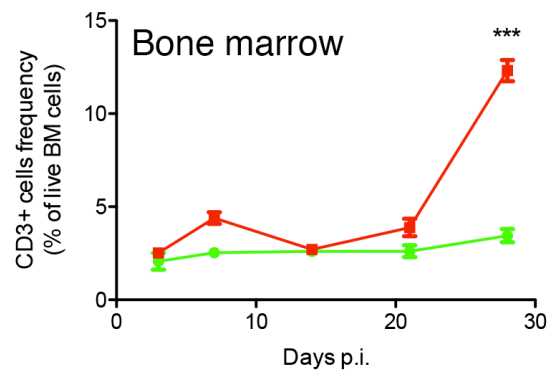
S2 Figure. Frequency of erythroid precursors in bone marrow.

Frequency of erythroid precursors (pro-erythroblasts and erythroblasts) in the bone marrow of naïve (green) and *L. donovani*-infected (red) B6 mice over time. Precursors were identified on the basis of TER119 and CD71 staining. Unpaired t-test; n=3 mice per group per timepoint).



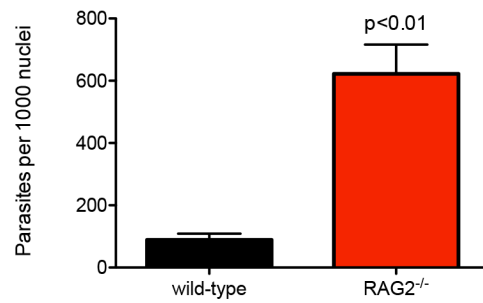
S3 Figure Myelogram of *L. donovani*-infected BM

BM samples were obtained by aspiration biopsy from iliac crest using 24 G needle attached to a 5mL disposable plastic syringe with 10% EDTA and smears were stained with May–Grünwald Giemsa and analyzed by optical microscopy (Zeiss, Germany) and images using Zen software (Carl Zeiss). A Binucleated erythroid cell. B Megalocyte. C. Atypical mitosis. D Emperipolesis.



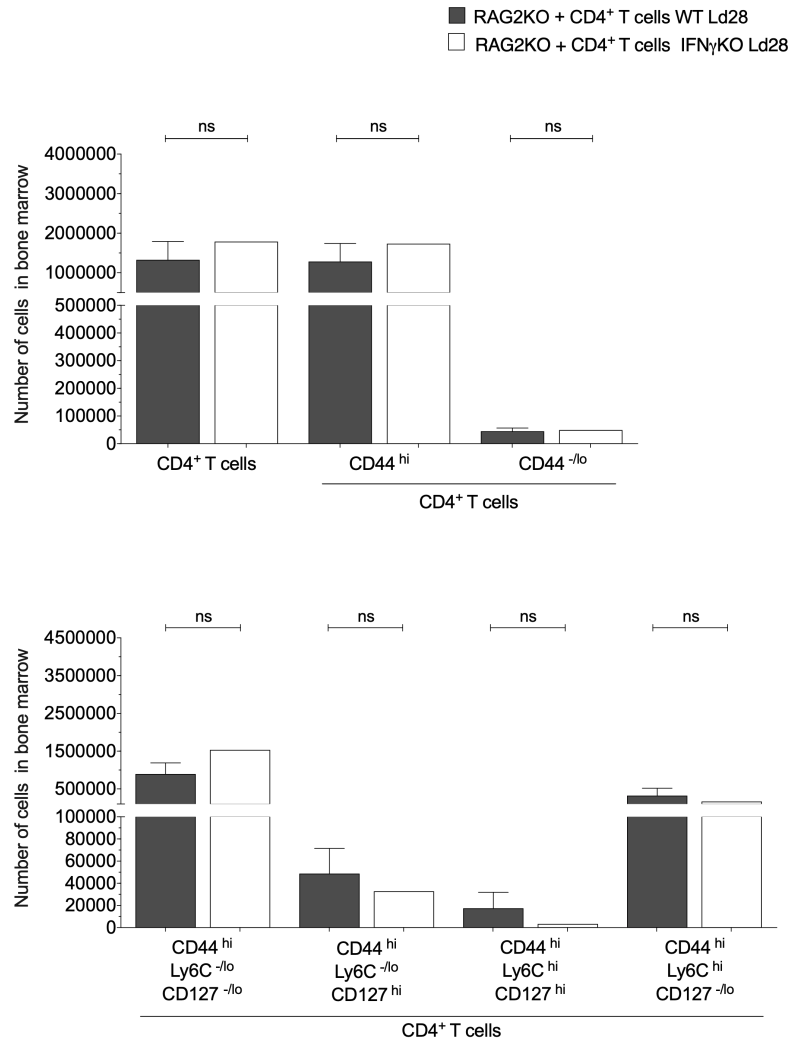
S4 Figure Frequency of T cells in bone marrow

Frequency of CD3⁺ cells in the bone marrow of naïve (green) and *L. donovani*-infected (red) B6 mice over time. Unpaired t-test; n=3 mice per group per timepoint).



S5 Figure. Parasite load in *L. donovani* infected B6 and B6.*Rag2*^{-/-} mice.

Parasites per 1000 nuclei in the spleen at d28 p.i.. Spleen impressions smears were made on glass slides and stained with Giemsa. Parasites and nuclei were counted microscopically. n=8 wild-type and 6 RAG2^{-/-} mice from 2 independent experiments.



S6 Figure. Number and differentiation state of wild type and IFN γ KO CD4⁺ T cells in RAG recipients.

Wild type (black bars) or IFN γ KO (open bars) CD4⁺ T cells were transferred into RAG recipients prior to infection with *L. donovani*. At day 28 p.i., BM CD4⁺ T cells were enumerated and characterized by flow cytometry. **A.** Number of total CD4⁺ T cells and of CD4⁺ T cells with CD44^{hi} and CD44^{lo} phenotype. **B.** Number of CD4⁺ T cells expressing different expression patterns for Ly6C, CD44 and CD127. CD44^{hi}Ly6C^{lo}CD127^{lo} are often regarded as classical effector cells. Two tibias and femurs were taken per mouse with n=4 mice receiving wild type T cells and n=5 mice receiving KO T cells.